

RESEARCH ARTICLE | FEBRUARY 06 2024

Rupture of membranous microbubbles induced by pulsed acoustic wave FREE

Menyang Gong (宫门阳)  ; Xin Xu (徐鑫)  ; Zhonghan Fei (费仲晗)  ; Yuanyuan Li (李媛媛);
Shenlian Gao (高沈廉); Yupei Qiao (乔玉配)  ; Jiehui Liu (刘杰惠); Teng Ma (马腾) ;
Xiaozhou Liu (刘晓宙) 



Physics of Fluids 36, 027111 (2024)

<https://doi.org/10.1063/5.0189850>



CrossMark



Physics of Fluids
Special Topic:
Flow and Civil Structures
Submit Today

AIP Publishing

Rupture of membranous microbubbles induced by pulsed acoustic wave

Cite as: Phys. Fluids 36, 027111 (2024); doi: 10.1063/5.0189850

Submitted: 1 December 2023 · Accepted: 12 January 2024 ·

Published Online: 6 February 2024



Menyang Gong (宫门阳),¹ Xin Xu (徐鑫),¹ Zhonghan Fei (费仲晗),¹ Yuanyuan Li (李媛媛),¹ Shenlian Gao (高沈廉),¹ Yupei Qiao (乔玉配),² Jiehui Liu (刘杰惠),¹ Teng Ma (马腾),^{3,a} and Xiaozhou Liu (刘晓宙)^{1,4,a}

AFFILIATIONS

¹Key Laboratory of Modern Acoustics, Institute of Acoustics and School of Physics, Collaborative Innovation Center of Advanced Microstructures, Nanjing University, Nanjing 210093, China

²School of Physics and Electronic Science, Guizhou Normal University, Guiyang 550001, China

³Shenzhen Institute of Advanced Technology, Chinese Academy of Sciences, Shenzhen 518055, China

⁴State Key Laboratory of Acoustics, Institute of Acoustics, Chinese Academy of Sciences, Beijing 100190, China

^aAuthors to whom correspondence should be addressed: teng.ma@siat.ac.cn and xzliu@nju.edu.cn

ABSTRACT

Encapsulated microbubbles serve as suitable drug carriers in medicine. This paper proposes corrections for the resonance frequency of lipid-coated bubbles under various acoustic pressure levels and the critical pressure for bubble rupture based on the Marmottant model. The suggestion to induce the rupture of lipid-coated bubbles using acoustic waves leans toward utilizing pulse waves rather than continuous waves. Corresponding experiments validate the accuracy of these corrections and the rationale behind the suggestion, aligning closely with theoretical predictions. This study offers a more precise predictive framework for the behavior of lipid-coated bubbles under acoustic waves.

Published under an exclusive license by AIP Publishing. <https://doi.org/10.1063/5.0189850>

10 February 2024 23:34:43

I. INTRODUCTION

Drugs are of great significance for relieving patients' suffering and increasing life expectancy. However, a considerable part of the drugs used for treatment is toxic to normal cells or has high chemical activity, which will degrade quickly in the body fluid environment. Previously, in order to avoid and reduce side effects and improve the efficiency of drug action, bio-targeted drugs based on biomarkers were developed.^{1–6} Through the specific recognition of cell membrane proteins, the drug can be more combined with the target cell. However, the conditions for the identification of biomarkers are very harsh, and it is difficult to form a general solution for the design of specific targeting groups for different drug molecules, which leads to the high cost of targeted therapy with biomarkers. Furthermore, in quite a few medical application scenarios, the lesions are relatively concentrated and appear as clusters in space, such as tumors, calculus, and other diseases.

Enveloped microbubbles have been proved to be suitable carriers for carrying drugs, and microbubbles based on phospholipid molecular layers have good stability and biocompatibility.^{7–9} Kooiman *et al.* delineated the dynamic lipid movements of fluorescently labeled lipid membrane bubbles under acoustic influence for the first time using high-speed cameras within the nanosecond timescale.¹⁰ Marmottant *et al.* predicted the impact of acoustic pressure pulses on bubbles, expressing the bubble's surface tension as a piecewise function.

It introduced a critical shell tension model leading to bubble rupture, known as the Marmottant model.¹¹ Minnaert comprehensively reviewed fundamental research on microbubbles and the advancements in drug delivery strategies utilizing microbubbles, highlighting pressing research challenges yet to be addressed.¹²

In recent years, acoustic manipulation has attracted widespread attention as a non-contact manipulation method suitable for life sciences.^{13–21} Not only nonlinear acoustic effects can manipulate particles, but also the enveloped microbubbles carrying drugs can be broken by the resonance effect of nonlinear acoustics.

This suggests that we can build a focused area of a specified frequency near the lesion. Patients only need to inject microbubbles containing drugs. The microbubbles in the focused area are continuously ruptured due to the acoustic resonance effect, where the drug is released. Due to the diffusion effect in the body fluid environment, the drug-carrying microbubbles will continue to diffuse to the vicinity of the lesion, thereby achieving a spatial targeting effect.

II. THEORY AND NUMERICAL CALCULATIONS

A. Process of spatially targeted drug release

Figure 1 schematically draws the realization process of spatial targeting. First, the drug-encapsulated microbubbles are injected into the body. After the microbubbles enter the body, based on the diffusion

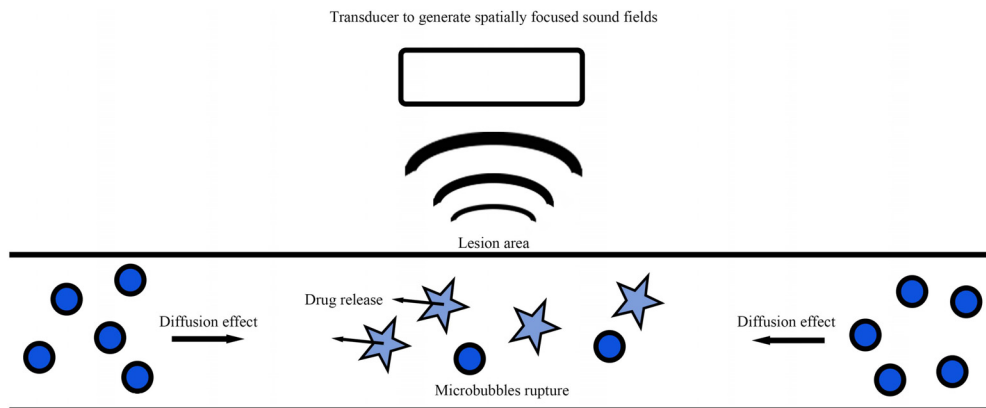


FIG. 1. Process of spatially targeted drug release.

effect, the microbubbles partially wrapped with the drug will diffuse to the vicinity of the lesion, as shown in Fig. 1. When a focused acoustic field of a specified frequency is applied near the lesion, the microbubbles encapsulating the drug will burst, and the drug will be released. As the concentration of microbubbles near the lesion decreases, the microbubbles in other areas are continuously replenished based on the diffusion effect, thereby the microbubbles continuously breaking near the lesion, and the spatial targeting effect is realized.

B. Resonant frequency of enveloped microbubbles

The size of common drug molecules is generally smaller than micrometers, and the diameter of capillaries is generally 6–9 μm . In order to better realize the diffusion effect in Fig. 1, it is appropriate to choose enveloped bubbles with a diameter of 3 μm or less. Based on drug loading and efficiency considerations, enveloped microbubbles with a radius size of 1.5 μm are selected. Due to its good biocompatibility, phospholipid molecules are selected as membrane materials for enveloped bubbles.

A phospholipid bubble does not have a fixed resonant frequency due to its strong nonlinearity of surface tension.²² The behavior of phospholipid bubbles can be described by the Marmottant model.¹¹ Based on this model, the vibration equation of phospholipid microbubbles can be expressed as

$$\rho_l \left(R \ddot{R} + \frac{3}{2} \dot{R}^2 \right) = \left[p_0 + \frac{2\sigma(R_0)}{R_0} \right] \left(\frac{R}{R_0} \right)^{-3\kappa} \left(1 - \frac{3\kappa}{c} \dot{R} \right) - \frac{2\sigma(R)}{R} - \frac{4\mu \dot{R}}{R} - \frac{4\kappa_s \dot{R}}{R^2} - p_0 - p_{ac}. \quad (1)$$

Here, ρ_l , p_0 , p_{ac} , R , and R_0 are the liquid density, the ambient pressure, the driving acoustic pressure, the bubble radius, and the original bubble radius, respectively. \dot{R} and \ddot{R} are the first and second time derivatives of R , respectively. $t_R = R/c$, where c is the sound speed in the environmental liquid. μ , κ_s , and κ are the viscosity of the surrounding liquid, the surface dilatational viscosity from the monolayer, and the polytropic gas exponent, respectively, which equals the ratio of specific heats for bubbles behaving adiabatically.²³

In the Marmottant model, the phospholipid coating of a bubble is regarded as a layer whose surface tension is close to zero when the

bubble shrinks while increases rapidly when the bubble grows bigger. The surface tension can be expressed as¹¹

$$\sigma(R) = \begin{cases} 0 & \text{if } R \leq R_{buckling}, \\ \chi \left(\frac{R^2}{R_{buckling}^2} - 1 \right) & \text{if } R_{buckling} \leq R \leq R_{break-up}, \\ \sigma_{water} & \text{if ruptured or } R \geq R_{ruptured}. \end{cases} \quad (2)$$

Here, $R_{buckling} = R_0 / \sqrt{1 + \sigma(R_0) / \chi}$ is the buckling radius, and $R_{break-up} = R_0 / \sqrt{1 + \sigma_{break-up} / \chi}$ is the rupture radius. $R_{ruptured} = R_0 / \sqrt{1 + \sigma_{water} / \chi}$ is the critical radius to maintain ruptured. χ is an elastic modulus that gives the slope of the bubble's surface tension in the elastic state.

In the Marmottant model, we consider the encapsulated bubble to always maintain a spherical shape, and rupture occurs when the bubble reaches its critical radius. Under the influence of acoustic waves, the radius of the encapsulated bubble undergoes periodic changes.¹¹ Equation (2) precisely defines the rupture condition of the encapsulated bubble, specifically when its radius reaches the critical value.

Because the bubble breaks up when its radius exceeds the critical radius $R_{break-up}$, the more violent the bubble oscillates, the easier it is to breakup. Normally, bubbles have the largest oscillating amplitude at their resonant frequency.

Numerical simulations are conducted by solving Eq. (1) using the fourth order Runge-Kutta method, and the parameters involved are based on references,^{11,24–26} as listed in Table I. Figure 2 shows the numerical calculated frequency-response curves of bubbles under different incident acoustic pressures based on Eq. (1), where the same parameters are used. R_{max} and R_{min} are the maximum and the minimum radius reached by the microbubble when the corresponding acoustic wave is applied. As the sound pressure increases, the resonance frequency shifts to lower frequencies.

In numerical simulations and experiments, microbubbles with a radius of 1.5 μm are selected. In order to find out the critical sound pressure amplitude for bubbles to breakup, the curve of the maximum radius during bubble oscillation with respect to the amplitude of the incident acoustic wave is plotted in Fig. 3. At 2.0 MHz, which is close to the resonant frequency of bubbles, the critical amplitude of acoustic

TABLE I. List of fixed parameters used in simulations.

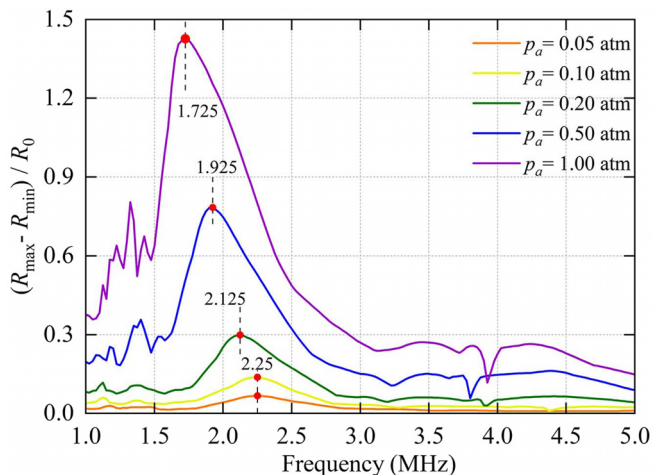
Parameters	Values
c	1.50×10^3 m/s
ρ_l	1.00×10^3 kg/m ³
μ	2.98×10^{-3} Pa · s
σ_{water}	7.29×10^{-2} N/m
$\sigma(R_0)$	1.00×10^{-3} N/m
$\sigma_{\text{break-up}}$	8.02×10^{-2} N/m
χ	2.00 N/m
κ_s	5.00×10^{-10} N
p_0	1.01×10^5 Pa
κ	1.095

pressure required for bubble's breakup is about 0.10 atm. We define p_{thres} as the critical sound pressure threshold above which the bubble radius will exceed $R_{\text{break-up}}$. When the sound pressure exceeds or reaches p_{thres} , the microbubbles will rupture to release the drug. When the sound pressure is below p_{thres} , microbubbles do not rupture, and the drug can be diffused and transported safely and stably.

It can be seen from Fig. 2 that the resonant frequency of phospholipid-coated microbubbles with an initial radius of 1.5 μm is around 2 MHz, so it is more appropriate to use 2 MHz sound waves to break down microbubbles. To test this idea, numerical calculations are further carried out. As shown in Fig. 3, when the sound wave frequency is 2 MHz, which is close to the resonant frequency, the sound pressure only needs to reach 0.10 atm to make the radius of the enveloped phospholipid bubbles reach the rupture radius, resulting in a rupture phenomenon to release the drug. At non-resonant frequencies, such as 1 and 3 MHz, the sound pressure needs to reach 0.18 or 0.30 atm to reach the rupture radius. While at the frequencies far away from resonance, this critical pressure becomes larger, suggesting more difficulty for bubbles to breakup.

C. Improvement scheme of incident sound beam

Since breaking the envelope bubbles requires a large sound field sound pressure, the output sound pressure of the transducer is quite large, and the continuous wave will produce an obvious thermal effect that can cause damage to biological tissues.^{27–30} The thermal effect here refers to the phenomenon that the sound energy in the sound

**FIG. 2.** Frequency-response curves of lipid microbubbles based on numerical calculations.

wave is converted into internal energy during the action, causing the temperature of the local area to increase. These thermal effects are generally detrimental during treatment. The thermal effect is related to the time integral of the acoustic energy flow, while the phenomenon of microbubble breaking is more related to the instantaneous sound pressure. Therefore, we have improved the continuous wave scheme and multiplied the rectangular wave function to the emission signal, thereby greatly reducing the thermal effect in the process without significantly affecting the effect of breaking the microbubbles.

III. EXPERIMENT

A. Environment construction and experiment steps

In order to verify whether the design scheme of the spatially targeted drug release process in theory can be applied in practice, the experiment of breaking enveloped microbubbles is carried out. As shown in Fig. 4, the experimental environment is set up. The microscope used in the experiment is Motic AE2000. An pool built by acrylic material is placed on top of the microscope platform. The pipes of plastic are fixed in the pool. The microbubbles used in the experiment are phospholipid microbubbles with an average radius of 1.5 μm . The shell of the microbubbles used in the experiment is composed of polyethylene glycol, distearoylphosphatidylcholine, dipalmitoylphosphatidylglycerol

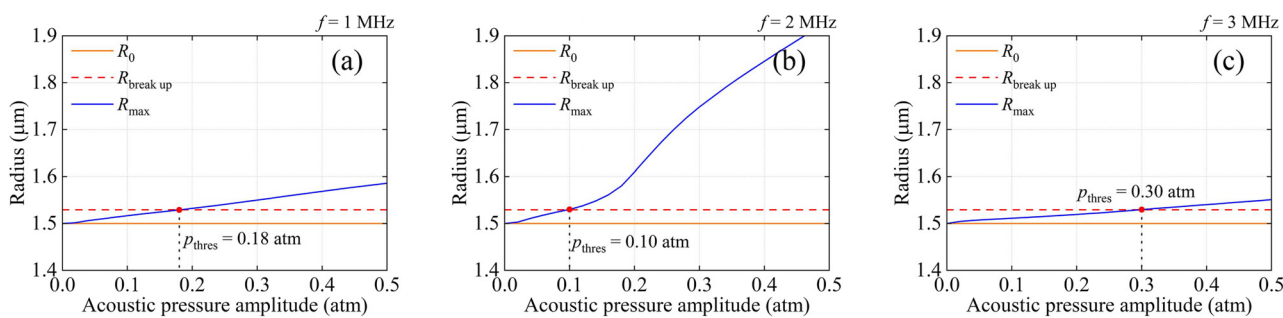
**FIG. 3.** The acoustic pressure threshold for bubble rupture at different frequencies of (a) 1.0 MHz, (b) 2.0 MHz, and (c) 3.0 MHz based on numerical calculations.



FIG. 4. Experimental setup.

sodium (DPPG.Na), and palmitic acid. The drug encapsulated inside the microbubbles is temporarily substituted with sulfur hexafluoride. This bubble material has been widely employed in medical contrast agents, and its adverse reactions have been verified to be mild, transient, self-reversible, and without residual effects. Hence, it serves as a suitable drug delivery carrier. The transducer is fixed on one side of the pipe by a universal clamp. If not specified, the transducer center frequency is 2 MHz. The signal generator model is Agilent 33250A, and the amplification factor of the power amplifier is 20 dB.

First, the pool is filled with distilled water to simulate the interstitial fluid environment. The coated microbubbles prepared with distilled water and uniformly diluted are injected into the pipeline, and it can be observed that there are a large number of coated microbubbles in the tube. Starting the signal generator and power amplifier, the transducer emits sound waves and forms a focused sound field with a specified frequency in the tube. The entire process of the experiment can be observed using a microscope. The sound pressure at the focused sound field is measured by hydrophone. In the de-ionized water medium, prior to injecting the bubbles, the water hydrophone is employed to conduct a preliminary experiment to measure the acoustic pressure distribution in the absence of bubbles. These data served as the parameter basis for the incident acoustic field.

B. Experimental phenomena

Under the action of the focused acoustic beam, the acoustic microbubbles are first subjected to the secondary Bjerknes force to aggregate into microbubble clusters because the vibration bubbles in the same phase will be agglomerated by the force.³¹ The microbubbles aggregated into clusters rupture, releasing the contained drug. The gas

contained in the acoustic microbubbles aggregates to form larger microbubbles. Clusters of microbubbles can be easily distinguished from larger microbubbles aggregated after microbubble collapse, as shown in Fig. 5. Larger microbubbles have apparent optical hollows under the microscope. However, microbubble clusters appear as continuous dark shadows. Therefore, the rate at which the acoustic microbubbles collapse can be measured by observing the time it takes for the acoustic microbubbles to coalesce into larger microbubbles.

First, the resonant frequency of the acoustic microbubbles is verified. 1, 2, and 3 MHz focused signals are used to break the acoustic microbubbles, respectively. The sound pressure at the focused sound field is 0.150 atm. As shown in Fig. 6, it can be seen that under the excitation of the 2 MHz focused acoustic beam, the acoustic microbubbles only need 15 s to aggregate and rupture. However, under the action of focused acoustic beams of 1 and 3 MHz, the acoustic microbubbles only aggregate due to the secondary Bjerknes force and do not rupture. This further verifies that the prediction of the resonant frequency in the theory is quite accurate using the Marmottant frequency. Under the excitation of the resonant frequency, the acoustic microbubbles can be broken, thereby realizing the release of the drug.

Furthermore, the experiments are conducted to verify the effect of different focused acoustic pressures on the rupture rate of acoustic microbubbles. As shown in Fig. 7, the focused sound pressures are 0.025, 0.075, 0.100, 0.125, and 0.150 atm. The frequency of the incident sound beam is the resonant frequency, which is 2 MHz. The acoustic pressure threshold for microbubble collapse in this case is predicted in theory to be 0.100 atm. It can be seen from the experiment that when the focused sound pressure does not reach 0.100 atm, the acoustic microbubbles will only gather into clusters without rupture. When the focused sound pressure reaches 0.100 atm, the acoustic microbubbles

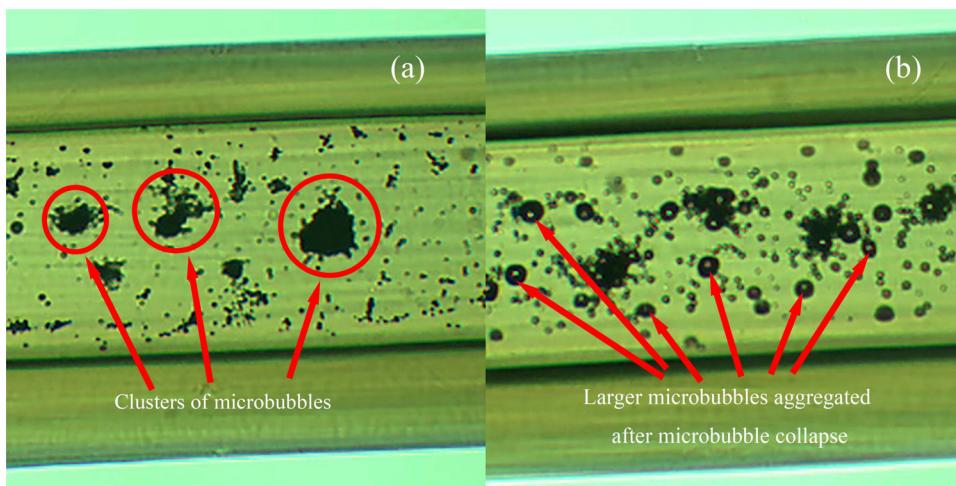


FIG. 5. Comparison of microbubble clusters and larger microbubbles aggregated after microbubble rupture. (a) Clusters of microbubbles. (b) Larger microbubbles aggregated after microbubble collapse.

begin to rupture, and the drug contained in them is released. This is in line with the prediction of the phenomenon in our theoretical calculations. As shown in Fig. 3, when the frequency of the focused sound beam is 2 MHz, the critical value of the breaking sound pressure is 0.100 atm. The greater the focused sound pressure, the faster the aggregation and rupture of the acoustic microbubbles. When the focused sound pressure reaches 0.150 atm, aggregation and rupture begin to appear when the transducer acts for 5 s. When the sound pressure is 0.125 atm, the same phenomenon cannot be observed until 15 s.

As stated in the theory, although increasing the focused acoustic pressure can increase the rate of microbubble aggregation and collapse, it brings deleterious thermal effects.^{27–30} The addition of a rectangular window to continuous sine waves results in transforming them into a series of sinusoidal pulse waves with time intervals. The purpose of

adding the rectangular window was to validate that the critical surface tension leading to bubble rupture primarily depends on the instantaneous intensity of the acoustic pressure rather than continuous exposure. Both the sinusoidal pulse waves depicted in Figs. 8–10 have a frequency of 2 MHz. As shown in Fig. 8, the width of the rectangular function is $2.5 \mu\text{s}$, exactly a group of five transmission cycles of 2 MHz. The period of the rectangular function used in the experiment is 5 and $2.5 \mu\text{s}$ (continuous sine wave). As shown in Figs. 9 and 10, it can be observed that when the period of the rectangular function is $5 \mu\text{s}$, the break rate is almost the same as that of the continuous sine wave. However, the output power is reduced by half, and the thermal effect is significantly suppressed in this way. This verifies the conjecture in the theoretical part that the bursting velocity of the microbubbles is sensitive to the instantaneous sound pressure, and the use of the rectangular

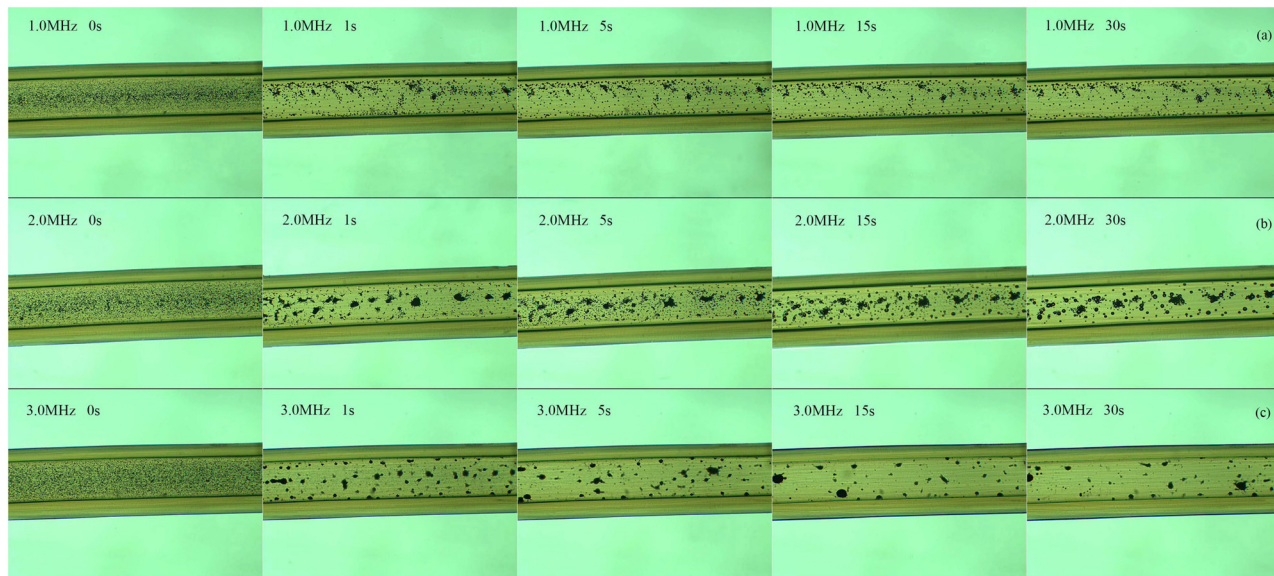


FIG. 6. The rupture of acoustic microbubbles under the action of (a) 1 MHz, (b) 2 MHz, and (c) 3 MHz focused sound waves.

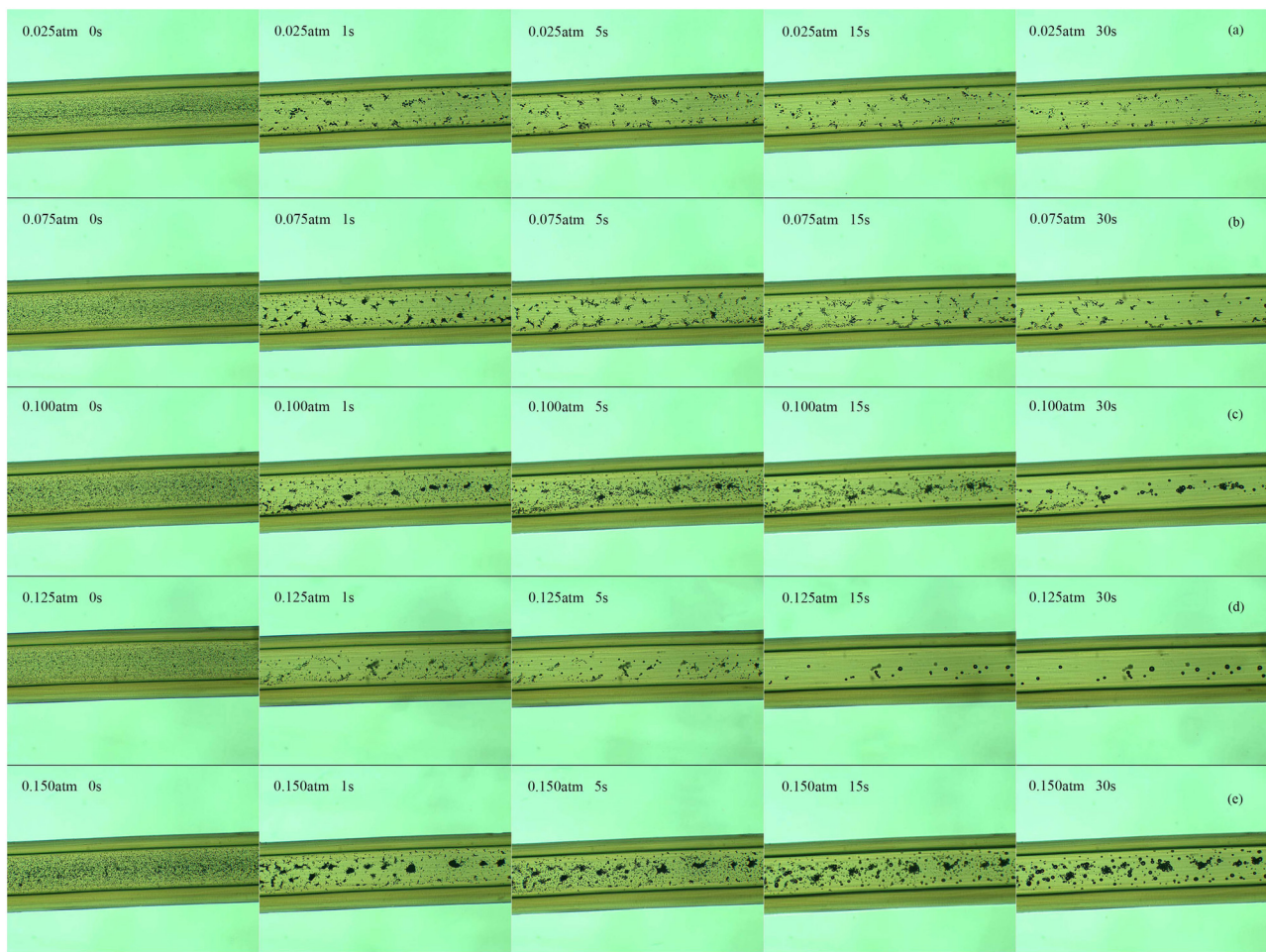


FIG. 7. Acoustic microbubble rupture under different sound pressures of (a) 0.025 atm, (b) 0.075 atm, (c) 0.100 atm, (d) 0.125 atm, and (e) 0.150 atm.

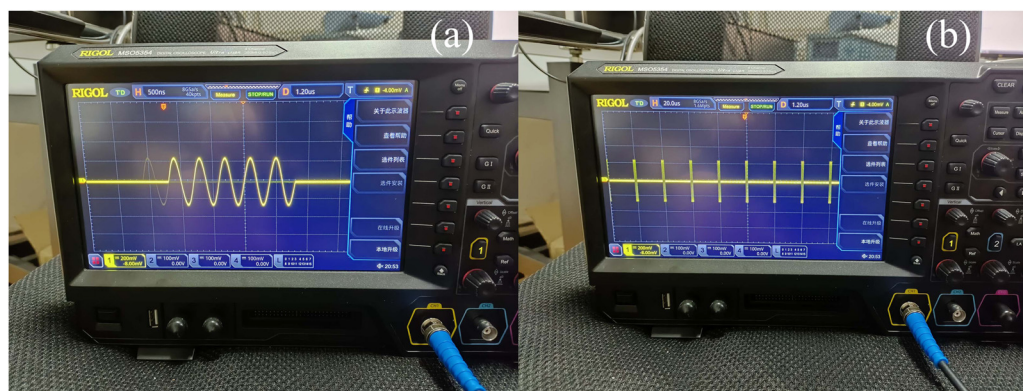


FIG. 8. (a) Continuous sine waves and (b) sinusoidal pulse waves with time intervals in experiment. The frequency of both the sinusoidal waveform and pulsed waveform is 2 MHz. The width of the sinusoidal pulsed waveform is $2.5 \mu\text{s}$.

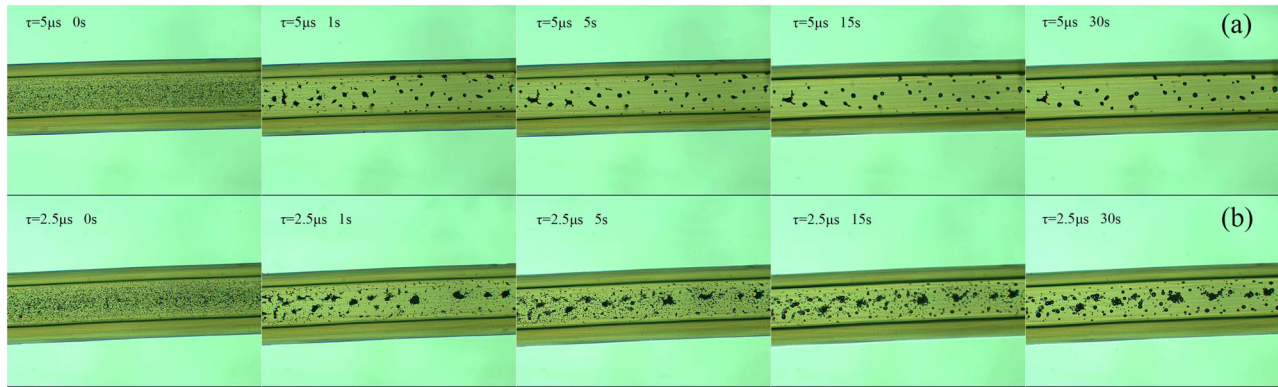


FIG. 9. The rupture of acoustic microbubbles under the action of continuous sine waves and sinusoidal pulse waves with time intervals in experiment. (a) $\tau = 5 \mu\text{s}$ and (b) $\tau = 2.5 \mu\text{s}$.

wave function does not have a large impact on the bursting rate of the microbubbles.

IV. DISCUSSION AND CONCLUSION

As outlined in this paper, our analysis of membrane bubbles is also grounded in the Marmottant model,¹¹ employing a piecewise function formulation, as per Eqs. (1) and (2). Previous studies largely overlooked the influence of varying acoustic pressures causing resonance frequency shifts in bubbles, as demonstrated in the Marmottant model.¹¹ However, the resonance frequency of bubbles within different incident acoustic pressures is not fixed. As depicted in Fig. 2's analysis, with increasing pressure, the bubble's resonance frequency should continuously shift toward lower frequencies, rather than remain at a fixed value. Following this correction, in Fig. 3, we predict the critical pressure for bubble rupture at different frequencies post-correction. Subsequent experiments (Fig. 7) validate the accuracy of this correction. Furthermore, attaining the critical surface tension for bubble rupture requires high acoustic pressures, resulting in noticeable thermal effects.^{27–30} The thermal effects of sound waves are associated with the time integral of sound energy

flow, while the critical surface tension required for bubble rupture is contingent on instantaneous acoustic pressure. Therefore, our theoretical proposition advocates the use of pulse waves instead of continuous waves to rupture bubbles as it should require a lower energy input. Subsequent experiments (depicted in Fig. 9) showcase nearly identical bubble rupture effects using pulse waves with a $5 \mu\text{s}$ time width and continuous waves. To summarize, the primary innovations in this paper compared to prior related works include: 1. Proposing corrections for the resonance frequency of bubbles under varying acoustic pressures and the critical pressure for bubble rupture, experimentally validating these corrections; 2. Suggesting the use of pulse waves rather than continuous waves for bubble rupture under acoustic waves and substantiating this recommendation through experimentation.

In this work, we propose a modification based on the Marmottant model for the resonant frequency and critical pressure of bubble collapse of coated microbubbles under different sound pressure levels. Proposal for using sound waves to induce bubble collapse in coatings favors the use of pulsed waves rather than continuous waves. Corresponding experiments verify the accuracy of the modification and suggestion, in close agreement with theoretical predictions. This study provides a more precise predictive framework for the behavior of coated microbubbles under sound waves. The space-targeted drug release process based on coated microbubbles proposes a new drug delivery method, which can effectively improve the efficiency of drug action and greatly reduce the damage of drugs to normal tissues, thereby reducing the pain of patients and improving the quality of life of patients. It could be widely used in medicine and life sciences. This scheme has important application prospects in the fields of medicine and life sciences.

ACKNOWLEDGMENTS

Project supported by the National Key R&D Program of China (No. 2020YFA0211400), the State Key Program of National Natural Science of China (No. 11834008), the National Natural Science Foundation of China (Nos. 12174192 and 12204119), the State Key Laboratory of Acoustics, Chinese Academy of Sciences (No. SKLA202210), the Key Laboratory of Underwater Acoustic Environment, Chinese Academy of Sciences (No. SSHJ-KFKT-1701),

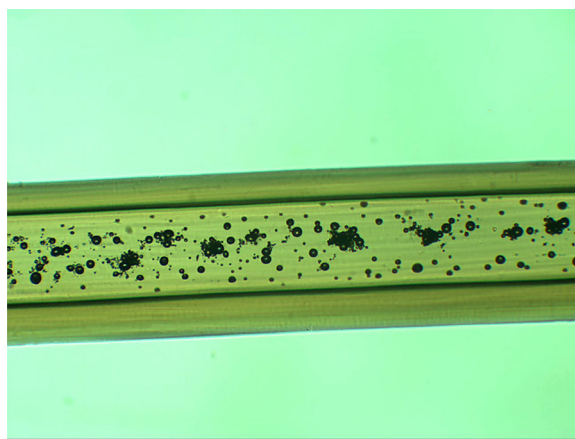


FIG. 10. The process video of the rupture of acoustic microbubbles under the action of sinusoidal pulse waves with time intervals. Multimedia available online.

and the Guizhou Provincial Science and Technology Foundation (No. ZK[2023]249).

AUTHOR DECLARATIONS

Conflict of Interest

The authors have no conflicts to disclose.

Author Contributions

Menyang Gong: Conceptualization (lead); Data curation (lead); Formal analysis (lead); Investigation (lead); Methodology (equal); Project administration (lead); Software (equal); Supervision (lead); Validation (lead); Visualization (lead); Writing – original draft (lead); Writing – review & editing (equal). **Xin Xu:** Methodology (equal); Software (equal). **Zhonghan Fei:** Methodology (supporting). **Yuanyuan Li:** Methodology (supporting). **Shenlian Gao:** Software (supporting). **Yupei Qiao:** Software (supporting). **Jiehui Liu:** Methodology (supporting). **Teng Ma:** Resources (supporting). **Xiaozhou Liu:** Funding acquisition (lead); Project administration (supporting); Resources (lead); Writing – review & editing (equal).

DATA AVAILABILITY

The data that support the findings of this study are available from the corresponding authors upon reasonable request.

REFERENCES

- ¹L. Harland and A. Gaulton, "Drug target central," *Expert Opin. Drug Discovery* **4**, 857–872 (2009).
- ²P. Kumari, B. Ghosh, and S. Biswas, "Nanocarriers for cancer-targeted drug delivery," *J. Drug Targeting* **24**, 179–191 (2016).
- ³A. Mahmud, X. B. Xiong, H. M. Aliabadi, and A. Lavasanifar, "Polymeric micelles for drug targeting," *J. Drug Targeting* **15**, 553–584 (2007).
- ⁴G. Padmanaban, V. A. Nagaraj, and P. N. Rangarajan, "Drugs and drug targets against malaria," *Curr. Sci.* **92**, 1545–1555 (2007).
- ⁵P. J. Tonge, "Drug-target kinetics in drug discovery," *ACS Chem. Neurosci.* **9**, 29–39 (2018).
- ⁶V. P. Torchilin, "Drug targeting," *Eur. J. Pharm. Sci.* **11**, S81–S91 (2000).
- ⁷Q. H. Pu, R. Spooner, and L. A. DeLouise, "Identifying drug resistant cancer cells using microbubble well arrays," *Biomed. Microdev.* **19**, 17 (2017).
- ⁸C. Mannaris and M. A. Averkiou, "Investigation of microbubble response to long pulses used in ultrasound-enhanced drug delivery," *Ultrasound Med. Biol.* **38**, 681–691 (2012).
- ⁹A. Presset, C. Bonneau, S. Kazuyoshi, L. Nadal-Desbarats, T. Mitsuyoshi, A. Bouakaz, N. Kudo, J. M. Escoffre, and N. Sasaki, "Endothelial cells, first target of drug delivery using microbubble-assisted ultrasound," *Ultrasound Med. Biol.* **46**, 1565–1583 (2020).
- ¹⁰K. Kooiman, T. Van Rooij, B. Qin, F. Mastik, H. J. Vos, M. Versluis, A. L. Klibanov, N. De Jong, F. S. Villanueva, and X. Chen, "Focal areas of increased lipid concentration on the coating of microbubbles during short tone-burst ultrasound insonification," *PLoS one* **12**, e0180747 (2017).
- ¹¹P. Marmottant, S. van der Meer, M. Emmer, M. Versluis, N. de Jong, S. Hilgenfeldt, and D. Lohse, "A model for large amplitude oscillations of coated bubbles accounting for buckling and rupture," *J. Acoust. Soc. Am.* **118**, 3499–3505 (2005).
- ¹²S. Roovers, T. Segers, G. Lajoinie, J. Deprez, M. Versluis, S. C. De Smedt, and I. Lentacker, "The role of ultrasound-driven microbubble dynamics in drug delivery: From microbubble fundamentals to clinical translation," *Langmuir* **35**, 10173–10191 (2019).
- ¹³M. Y. Gong, Y. P. Qiao, Z. H. Fei, Y. Y. Li, J. H. Liu, Y. W. Mao, A. J. He, and X. Z. Liu, "Non-diffractive acoustic beams produce negative radiation force in certain regions," *AIP Adv.* **11**, 065029 (2021).
- ¹⁴M. Y. Gong, Y. P. Qiao, J. Lan, and X. Z. Liu, "Far-field particle manipulation scheme based on x wave," *Phys. Fluids* **32**, 117104 (2020).
- ¹⁵M. Y. Gong, M. J. Shi, Y. Y. Li, X. Xu, Z. H. Fei, Y. P. Qiao, J. H. Liu, A. J. He, and X. Z. Liu, "Resonant adhesion structure makes negative acoustic radiation force," *Phys. Fluids* **35**, 057108 (2023).
- ¹⁶M. Y. Gong, X. Xu, Z. H. Fei, Y. Y. Li, T. Liu, S. L. Gao, J. H. Liu, A. J. He, and X. Z. Liu, "Non-invasive manipulation scheme of spherical particle in viscous fluids in a tube based on acoustic radiation force," *J. Acoust. Soc. Am.* **153**, 812–820 (2023).
- ¹⁷M. Y. Gong, X. Xu, Y. P. Qiao, Z. H. Fei, Y. Y. Li, J. H. Liu, A. J. He, and X. Z. Liu, "Scheme of non-contact manipulation: Acoustic radiation force on spherical particle in a spherical shell structure," *Results Phys.* **46**, 106264 (2023).
- ¹⁸J. F. Li, A. Crivoi, X. Y. Peng, L. Shen, Y. J. Pu, Z. Fan, and S. A. Cummer, "Three dimensional acoustic tweezers with vortex streaming," *Commun. Phys.* **4**, 113 (2021).
- ¹⁹M. L. Palmeri and K. R. Nightingale, "Acoustic radiation force-based elasticity imaging methods," *Interface Focus* **1**, 553–564 (2011).
- ²⁰Y. P. Qiao, M. Y. Gong, H. B. Wang, J. Lan, T. Liu, J. H. Liu, Y. W. Mao, A. J. He, and X. Z. Liu, "Acoustic radiation force on a free elastic sphere in a viscous fluid: Theory and experiments," *Phys. Fluids* **33**, 047107 (2021).
- ²¹M. Rajabi and A. Mojahed, "Acoustic radiation force control: Pulsating spherical carriers," *Ultrasonics* **83**, 146–156 (2018).
- ²²A. A. Doinikov, J. F. Haac, and P. A. Dayton, "Resonance frequencies of lipid-shelled microbubbles in the regime of nonlinear oscillations," *Ultrasonics* **49**, 263–268 (2009).
- ²³A. Prosperetti, "Acoustic cavitation series.2. Bubble phenomena in sound fields.1," *Ultrasonics* **22**, 69–78 (1984).
- ²⁴X. Xu, M. Y. Gong, and X. Z. Liu, "Theoretical prediction of the scattering of spherical bubble clusters under ultrasonic excitation," *Ultrason. Sonochem.* **94**, 106308 (2023).
- ²⁵A. JafariSojahrrood, L. Nieves, C. Hernandez, A. Exner, and M. C. Kolios, "Theoretical and experimental investigation of the nonlinear dynamics of nanobubbles excited at clinically relevant ultrasound frequencies and pressures: the role of lipid shell buckling," *2017 IEEE International Ultrasonics Symposium (IUS)* (IEEE, 2017).
- ²⁶A. J. Sojahrrood, R. Earl, H. Haghi, Q. Li, T. M. Porter, M. C. Kolios, and R. Karshafian, "Nonlinear dynamics of acoustic bubbles excited by their pressure-dependent subharmonic resonance frequency: Influence of the pressure amplitude, frequency, encapsulation and multiple bubble interactions on over-saturation and enhancement of the subharmonic signal," *Nonlinear Dyn.* **103**, 429–466 (2021).
- ²⁷E. Maloney and J. H. Hwang, "Emerging HIFU applications in cancer therapy," *Int. J. Hyperthermia* **31**, 302–309 (2015).
- ²⁸R. Illing, J. Kennedy, F. Wu, G. Ter Haar, A. Protheroe, P. Friend, F. Gleeson, D. Cranston, R. Phillips, and M. Middleton, "The safety and feasibility of extracorporeal high-intensity focused ultrasound (hifu) for the treatment of liver and kidney tumours in a western population," *Br. J. Cancer* **93**, 890–895 (2005).
- ²⁹J. Barkin, "High intensity focused ultrasound (HIFU)," *Can. J. Urol.* **18**, 5634 (2011).
- ³⁰H. J. Jang, J.-Y. Lee, D.-H. Lee, W.-H. Kim, and J. H. Hwang, "Current and future clinical applications of high-intensity focused ultrasound (HIFU) for pancreatic cancer," *Gut Liver* **4**, S57 (2010).
- ³¹A. A. Doinikov, "Effects of the second harmonic on the secondary Bjerknes force," *Phys. Rev. E* **59**, 3016–3021 (1999).